Formation of Au-Si eutectic on silicon surface

Anna Lisa Pinardi

March 2008

Phas4201 - Final year Physics Project
Supervisor: Prof. Ian Robinson
Second supervisor: Prof. Des McMorrow

Abstract

In September 2007 an experiment on a Si(100) sample with a Au film around 40Å thick deposited on top was carried out under Ultra High Vacuum at the European Synchrotron Radiation Facility in Grenoble. The measurements mainly involved x-ray diffraction techniques to probe the behaviour of the surface as the temperature was changed and increased above the eutectic melting point. The study of such eutectic has a very high technological importance for applications such as the growth on nanowires. The presence of a highly reproducibe crystalline layer sitting on top of a liquid surface was observed, confirming previous literature.

Contents

1 Introduction **3**
- 1.1 Introduction to x-ray diffraction . . . 3
- 1.2 Properties of a eutectic and some of its applications . . . 7
- 1.3 Previous results by Oleg G. Shpyrko . . . 9

2 The experiment **12**

3 The Reflectivity **14**
- 3.1 Background information . . . 14
- 3.2 Results . . . 16
- 3.3 Error analysis . . . 19

4 Crystal Truncation Rods **21**
- 4.1 Introduction to CTR . . . 21
- 4.2 Observations . . . 23
  - 4.2.1 Gold powder rings . . . 23
  - 4.2.2 Roughness . . . 26
- 4.3 Calculations for fits . . . 28
  - 4.3.1 Manual fits . . . 29
  - 4.3.2 Fits with ANAROD . . . 34

5 Grazing Incident Diffraction **37**
- 5.1 Background information . . . 37
- 5.2 Results . . . 38
- 5.3 Error analysis . . . 42

6 Auger scans **44**

7 Further observations **48**

8 Discussion **50**

9 Conclusion **56**

10 Acknowledgements **57**

11 Bibliography **58**

1 Introduction

The first section of my report aims to justify the motivations and the purposes of carrying out an experiment on an AuSi eutectic under UHV conditions, and it also provides some background information essential to understand the analysis of the measurements.

We were inspecting a Si(100) sample with a very thin layer of gold evaporated on top, using x-ray diffraction techniques provided by the European Synchrotron Radiation Facility in Grenoble, France.

1.1 Introduction to x-ray diffraction

X-rays are widely used to probe the structure of materials, due to the fact that their wavelength is of the order of 1 Å, hence comparable in size with the interatomic and intermolecular spacings. Nowadays, the most important source of x-rays is synchrotron radiation, widely used for its brightness and for the very high energies (short wavelengths) attainable.

The simplest base of diffraction theory comes from Bragg's law. Consider an x-ray beam with wavevector $\vec{k}_I$ incident on a crystal.

Assuming a crystal to be constructed by an infinite array of planes of atoms separated by a distance d (as seen in Figure 1), the incident x-rays will be diffracted by this set of planes allowing for constructive or distructive interferences. The condition for achieving constructing interferences is given by Bragg's law:

$$2s\sin(\theta) = n\lambda \tag{1}$$

The momentum transfer $\vec{Q}$ defined in Figure 1 in elastic scattering is given by:

$$\vec{Q} = \vec{k}_F - \vec{k}_I \tag{2}$$

Elastic scattering implies diffraction with no energy loss, hence the magnitude of the initial and final wavevectors does not change:

$$\left|\vec{k}_I\right| = \left|\vec{k}_F\right| = k = \frac{2\pi}{\lambda} \tag{3}$$

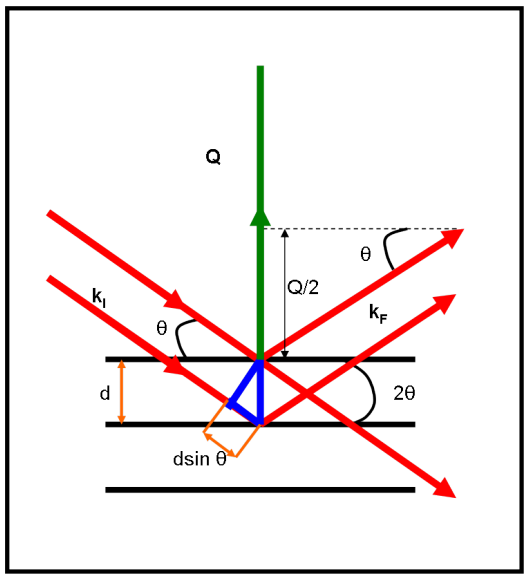

Figure 1: **Simple scattering diagram** - A beam of x-rays $\vec{k}_I$ (red arrows) incident at an angle θ on the sample is scattered by a set of planes: the diffracted beam may interfere constructively or distructively according to Bragg's law. The distance d indicates the distance between planes. The green arrow shows the momentum transfer $\vec{Q}$.

Using Equation 3 together with some simple trigonometry from Figure 1 a definition for a (scalar) momentum transfer is obtained:

$$Q = 2k \sin\theta = \frac{4\pi}{\lambda} \sin\theta \tag{4}$$

An ideal crystal is defined by an infinite lattice (a mathematical representation of its symmetry) plus a basis (the chemical component which is repeated along the lattice sites). A crystal is therefore an infinite periodic array with a constant chemical composition and constant structure. Its smallest representation is a unit cell defined by three lattice vectors $\vec{a_1}$, $\vec{a_2}$ and $\vec{a_3}$, and within this unit cell the distance from the origin to any point is defined (in Cartesian coordinates) by the vector:

$$\vec{r_j} = x_j\vec{a_1} + y_j\vec{a_2} + z_j\vec{a_3} \tag{5}$$

When discussing x-ray diffraction it is useful to define a reciprocal space to visualise the crystal, a space defined by the momentum transfer. The

reason for this is that the diffraction pattern of a crystal is easily represented by its own reciprocal lattice.

The reciprocal lattice vectors are defined by the following identity:

$$\vec{a_i^*} = \frac{2\pi \vec{a_j} \times \vec{a_k}}{\vec{a_i} \cdot (\vec{a_j} \times \vec{a_k})} \tag{6}$$

In reciprocal space, the vector corresponding to $\vec{r_j}$ (see Equation 5) is called the reciprocal lattice vector and is defined by:

$$\vec{G} = H\vec{a_1^*} + K\vec{a_2^*} + L\vec{a_3^*} \tag{7}$$

In Equation 7, H, K and L are integers called Miller indices.

Max von Laue in the early years of the 20^{th} century derived a new condition for x-ray diffraction, consistent with Bragg's law. He assessed that in order to observe constructive interference, the following condition has to be obeyed:

$$\vec{Q} = \vec{G} \tag{8}$$

This is called the Laue conditions, and from here we can obtain a value for the scalar momentum transfer Q in terms of the Miller indices for a cubic crystal. The reciprocal vector lattices of a cubic crystal are related to the lattice vector in real space by:

$$\vec{a_i^*} = \frac{2\pi}{a}\vec{a_i} \tag{9}$$

Combining Equation 9 with Laue condition (Equation 8) and the definition of $\vec{G}$ (Equation 7) the scalar momentum transfer for a cubic crystal becomes:

$$\left|\vec{Q}\right| = \frac{2\pi}{a}\sqrt{H^2 + K^2 + L^2} \tag{10}$$

Since for a cubic lattice the direction of the real space lattice vectors is equivalent to the one of the reciprocal lattice vectors, an expression for the

momentum transfer perpendicular to the crystal (z direction in real space) is found:

$$Q_{\perp} = \frac{2\pi}{a} L \tag{11}$$

Laue condition is also allows us to define the structure factor for a unit cell:

$$F = \sum_j f_j e^{-i\vec{G}\cdot\vec{r_j}} \tag{12}$$

By solving for the dot product $\vec{G}\cdot\vec{r}_j$, an expression for the structure factor in terms of the Miller indices is obtained:

$$F_{HKL} = \sum_j f_j e^{-i2\pi(x_j H + y_j K + zjK)} \tag{13}$$

The form factor f_j is defined as the Fourier transform of the electron density for a single atom, and it is different for every element. In x-ray scattering is often assumed to be equal to Z (the atomic number of an element), even though it is actually known to not be constant but to change as a function of Q.

The structure factor is a mathematical tool which defines the structure of a crystal and it is related to the amplitude of the scattered beam, whose square is equal to the intensity of the wave measured by the detector of any experiment:

$$I = |A|^2 \propto |F|^2 \tag{14}$$

The total amplitude of a scattered x-ray is equal to the convolution of the lattice part and the basis part. Equation 14 is a very simple relation which tells us how a scattered beam gives us information about the structure of the crystal: by finding a good fit to the measured intensity, the structure factor is automatically related to this fit, hence the strusture can be inferred.

Take for instance a Face-Centred Cubic crystal, a crystal with a four atom basis at $(x_j, y_j z_j) = (000)$, $\left(\frac{1}{2}\frac{1}{2}0\right)$, $\left(\frac{1}{2}0\frac{1}{2}\right)$, $\left(0\frac{1}{2}\frac{1}{2}\right)$. Substituting these values in Equation 13 the structure factor of a FCC crystal is obtained:

$$F_{FCC} = f\left(1 + e^{-i\pi(H+K)} + e^{-i\pi(K+L)} + e^{-i\pi(L+H)}\right) \tag{15}$$

The Miller indices are integers, hence there exist some selection rules for which for some value of HKL a zero structure factor is obtained. Physically, this means that no intensity is detected for that given Bragg peak, hence contribution from different atoms cancel out interfering distructively preventing the observation of a Bragg peak. For a FCC crystal, a Bragg peak is seen only if the Miller indices are either all odd or all even. If even only one index does not match this criterion, a destructive interference (no output of intensity) is observed.

More information on x-ray diffraction techniques can be found in references [1], [2] and [3].

1.2 Properties of a eutectic and some of its applications

In order to understand better the purposes of the experiment we first need to discuss briefly the properties of a eutectic.

A eutectic is simply a mixture of two elements at such proportions that its melting point is at the lowest possible temperature, much lower than the melting point of either of the two elements that make it up. For instance, gold melts at T_m=1063°C [7], silicon at T_m=1414°C [7], and the eutectic temperature for these two elements is T_E=359°C [4], more than 1000°C lower than the one of silicon.

To get a melting temperature as low as possible the two elements have to rearrange so that they reach a favourable relative concentration. The phase diagram of an Au-Si eutectic is given in Figure 2, and it shows that an AuSi alloy must contain 18% silicon and 82% gold to reach the liquid state at the lowest possible temperature.

The fact that the presence of another element lowers the melting point is a consequence of the increased entropy of the system: such system has 'extra' entropy coming from the fact that the atoms are different. Therefore the Gibb's free energy is lowered and the alloy is able to melt at a lower temperature than the pure element.

Eutectics are very important in technology. Since it is usually much easier to melt an eutectic than an element, they are often used for soldering,

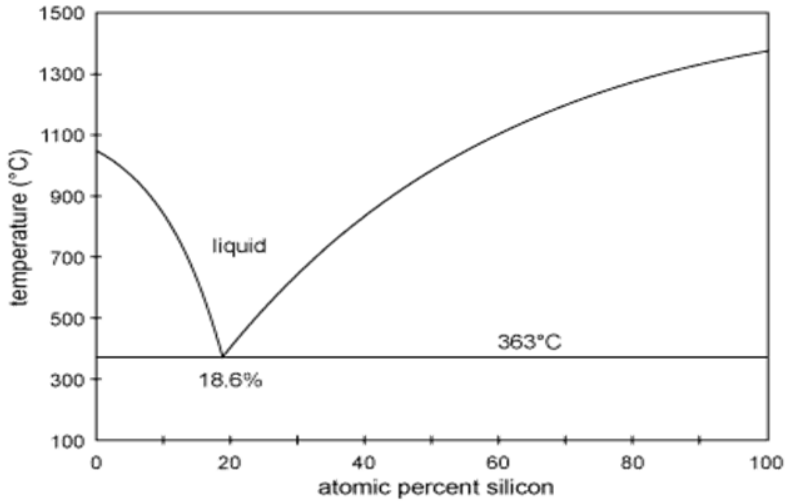

Figure 2: **Au-Si eutectic phase diagram** - This diagram shows that the lowest possible melting point for this system happens at 359°C [8].

where a liquid metal is used to make an electrical contact. This eutectic is particularly crucial because gold and silicon are often combined in electronic devices.

Moreover, eutectics are increasingly relevant in the creation of nanowires and nanotechnologies and they are often used as catalysts to help and fasten their growth. The dimensions of a nanowire are so small that the behaviour of atoms at the very surface becomes considerably important in determining the properties of such systems.

An example of a practical application of a eutectic is the Vapour Liquid Solid (VLS) method to grow nanowires. The set up is the following: at a fixed temperature higher than T_E, there is an isolated environment with a substrate and some gold drops with the diameter of a few nm on top of it. With the use of the Chemical Vapour Deposition (CVD) technique, a gas containing silicon (usually silane SiH_4) is introduced in the environment. This gas deposits on the substrate and also on the gold drops: hence since the temperature is high enough, gold and silicon form a eutectic liquid. If the gas keeps being introduced in the chamber, gold will reach saturation and silicon cannot penetrate the drops and form liquid anymore. Hence it starts to precipitate in solid form below the liquid tip, and a nanowire is created.

This is shown as a sketch in Figure 3.

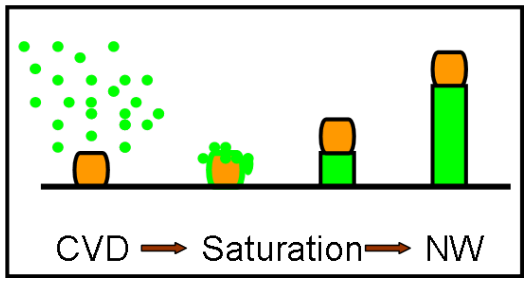

Figure 3: **VLS creation of a nanowire** - This sketch explains schematically the creation of a NW via VLS technique, starting from CVD, followed by the saturation and then by the growth of nanowire.

This technique is called VLS since it uses a vapour as a source of material to create a nanowire and a liquid eutectic as a catalyst in order to create a solid silicon nanowire.

1.3 Previous results by Oleg G. Shpyrko

Another experiment on an AuSi sample was carried out at the Argonne National Laboratory by Oleg G. Shpyrko and his team, and it was successively repeated at Brookhaven National Laboratory in order to confirm the results.

The sample was an alloy composed by 100 g of a mixture containing 18 % of silicon and 82 % gold. It was heated up above the eutectic temperature under Ultra High Vacuum conditions, and what was observed was very new, it had never been measured previously in similar systems.

First of all, an in-plane crystalline monolayer was detected at the very surface on the liquid sample, together with the presence of around six to eight atomic layers of a more ordered structure parallel to the surface, although not crystalline because of their lateral disorder.

This phenomenon in shown in Figure 4, and we can clearly see a broad liquid peak coming from a typical short-range ordering, together with some very sharp narrow surface Bragg peaks, originating from the solid nature of the surface.

The term 'surface freezing' indicates the presence of a crystalline surface sitting on top of a liquid sample. This circumstance was never observed before this experiment on a molten metallic alloy. This phenomenon though does not have to be confused with the usual two-three atomic layers ordered

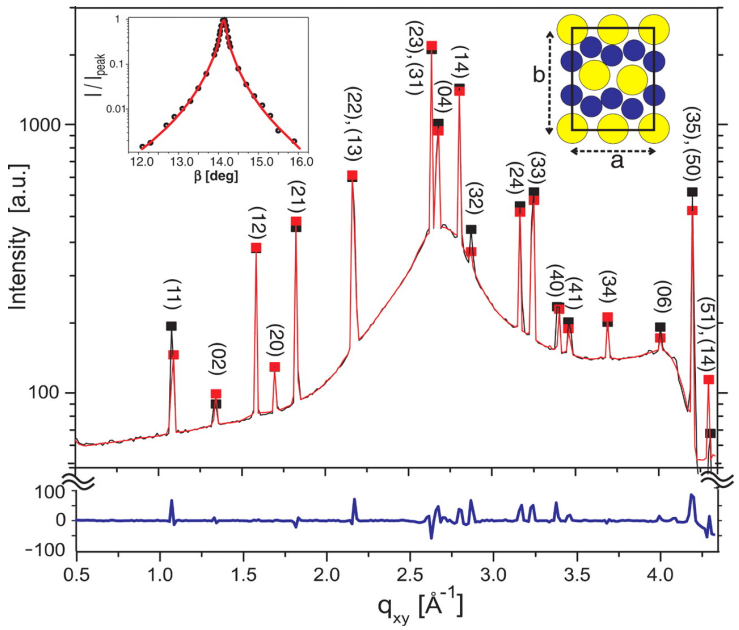

Figure 4: **Results by O. Shpyrko** - This figure shows the evidence for a surface crystalline layer on top of a liquid sample.

parallel to the surface, very often present in liquid metals just above the melting point: these last observations are indeed very common. However, Shpyrko assesses that in this case the length of this type of ordering is three-fold greater than usually observed (i.e. around 8 atomic layers).

The second important discovery revealed by his research is the presence of a solid surface first-order phase transition on increasing the temperature of the (molten) sample above 371°C.

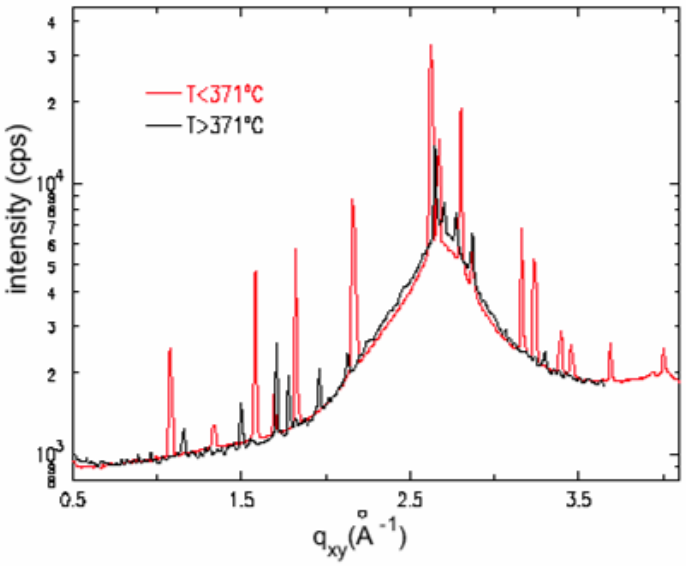

Figure 5: **Results by O. Shpyrko, phase transition** - This figure shows the surface phase transition, represented as a shift in momentum transfer of the peaks

This transition is shown in Figure 5 and is observed as a shift in the position of the surface peaks with respect to the momentum transfer q_{xy}.

One of the reasons for which the experiment Si-1419 was carried out at the ESRF was to reproduce and confirm the measurements assessed above obtained by Shpyrko.

For further and more detailed information see references [4] and [5].

2 The experiment

The experiment Si-1491 was carried out in September 2007 at ID03, the surface beamline, at the European Synchrotron Radiation Facility in Grenoble, France.

A Si(100) sample was fixed onto a ceramic insulated sample holder by two tantalum clips. The clips were linked to a power supply so that current could pass through them and heat up the sample. A thermocouple was also attached to the clips, in order to keep track of the temperature changes.

The sample was then introduced in a Ultra High Vacuum chamber, in order to ensure a clean environment with a pressure of the order of 10^{-10} mbar.

Pure silicon in open air is protected by a thin layer of oxides which prevents contamination from any other material, hence once introduced in the UHV chamber silicon was carefully cleaned by increasing the temperature adjusting the current passing through the clips. This way, the oxide layer would evaporate and be eliminated by the pumps attached to the UHV chamber. The highest temperature reached was 949°C on the thermocouple.

Some scans were taken on the pure silicon sample: a x-ray beam of energy E = 18 keV ($\lambda = 0.689$Å) was shone on the sample and different elastic scattering measurements were taken with several diffraction techniques allowed by the synchrotron source. Successively, few monolayers of gold were evaporated on top of the cold silicon using an ordinary evaporator attached to the chamber.

The temperature was then increased slowly from room temperature in steps of around 5-30°C up to 473°C, well above the eutectic temperature. The sample was hence observe to become liquid at the interface. Note that only the interface where silicon came to contact with gold became liquid due to eutectic properties: the bulk of the sample remained solid due to its very high melting point.

The sample was cooled down and heated up once again, in order to investigate the reproducibility of the observations. The temperature was then decreased to room temperature in order to allow for a new evaporation of extra gold on top of the sample. The new sample was then heated up above T_E and cooled down again.

Changes on the sample were tracked by different techniques involving x-ray diffraction, such as measurements on the reflectivity, crystal truncation rod scans and grazing incident diffraction observations. Some Auger scans

were also taken. Each of these technique aimed to track and analyse a different aspect of the sample, and they will be discussed in the next sections. Moreover, some SEM images of the sample after the manipulation were taken at the LCN successively, in November 2007.

Figure 6 shows a side view and a top view of the diffraction environment, defining some angles.

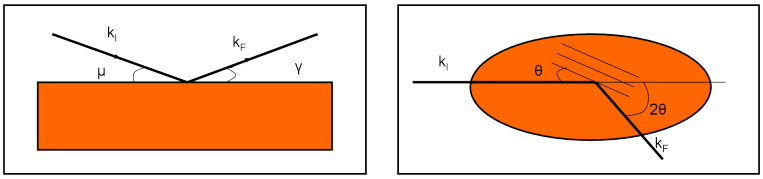

(a) Side view (b) Top view

Figure 6: **A (very) simplified sketch of the diffraction geometry of the experiment**

The angle of incidence is called μ and the diffraction angle is θ. The sample was allowed some freedom in inclination, and many other degrees of freedom were present, but they are not included in the Figure for simplicity.

3 The Reflectivity

Measurements on the reflectivity of a crystalline sample covered by a thin film such as in our experiment are often used to measure the thickness of the film. This section explains breafly how is this possible, and shows the results obtained together with error analysis for the thickness of the film.

3.1 Background information

The reflectivity is a measure of the ratio between the amplitude of the reflected wave to the incident wave. X-rays are scattered by the electrons in a material and it is therefore closely related to the electron density.

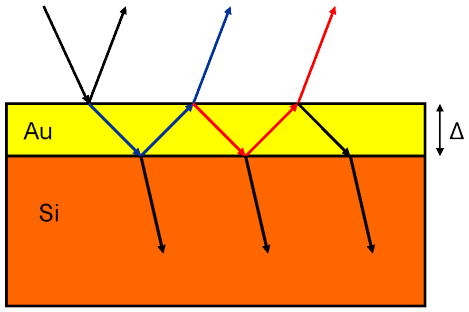

Figure 7: **Reflectivity from a thin film** - In this sketch the gold film (thickness Δ) is shown as a yellow slab on top of the silicon. A fraction of the incident x-ray (black) penetrates the film and a fraction of it is reflected; then when the AuSi boundary is reached the same thing happens: some wave is reflected and some goes through, and so on. This procedure is what gives rise to the contribution of the film to the total reflectivity which allows us to calculate the thickness of the film evaporated.

.

Figure 7 is a sketch of the behaviour of the incident ray: the presence of the gold film creates an extra Au-Si interface at which some of the incident x-ray is reflected and this fact give an extra contribution to the total measured reflectivity. Each contribution is shifted by a phase factor

$$p = e^{iQ\Delta} \tag{16}$$

where Δ indicates the thickness of the film and Q is the momentum transfer as defined in Equation 4. The different possible contributions add

up to form a geometric series so that the total reflectivity from the film becomes:

$$r_{film} = r_{01}\frac{(1-p^2)}{1-r_{01}p^2} \tag{17}$$

where r_{01} is the first contribution.

The reflectivity of the film is therefore related to the phase factor and hence to the thickness of the film (see Equation 16). The detector measures the intensity of the reflected beam, so referring to Equation 14, what is observed is simply the modulus square of the amplitude reflectivity (called the intensity reflectivity). The consequence of the phase shift due to the presence of the film is to create oscillations in the plot of the reflectivity against momentum transfer Q (see Figure 8). In our case, the reflectivity plots are is shown in terms of the diffraction angle θ, but this is closely related to the momentum transfer (see Equation 4).

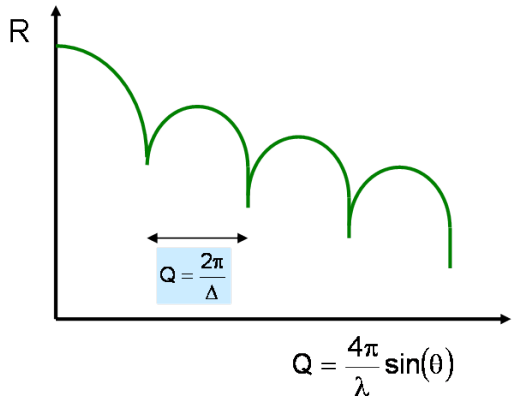

Figure 8: **Sketch of Reflectivity plot** - This diagram shows that the contribution of the film to the total reflectivity gives rise to oscillations, whose width is related to the thickness of the film.

The width of these oscillations is related to the thickness because

$$\Delta Q = \frac{2\pi}{\Delta} \tag{18}$$

Here ΔQ indicates the width of the oscillations in the plot. Hence, from Equation 4 and Equation 18, we can find a final expression for the thickness of the film Δ:

$$\Delta = \frac{\lambda}{2\sin(\theta_2 - \theta_1)} \tag{19}$$

Here λ indicates the wavelength of the incident x-rays, i.e. 0.689 Å. The difference in θ is what is manually obtained from the scans in order to get a good value for the thickness of the film, and these calculations are shown in the next section. For further details on the Reflectivity see Chapter 3 of [1].

3.2 Results

The first reflectivity scan was done just after the gold deposition and this is what will enable us to infer a first value of the thickness of the sample. Figure 9 shows the measurement I just described.

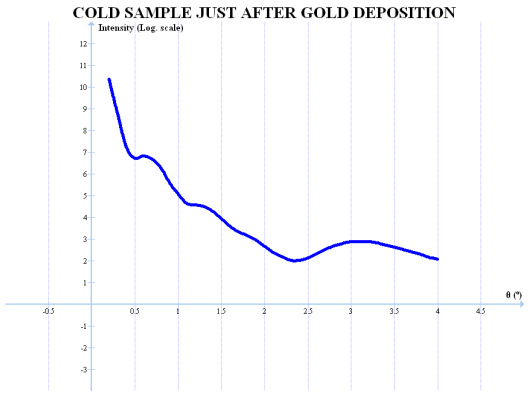

Figure 9: **First reflectivity measurement on cold sample, just after gold deposition** - Some oscillations are clearly seen in this scan, so that the thickness can be easily calculated.

The oscillations are clear, and hence the value of the diffraction angle for four minima was obtained at:

$$\theta_{min1} = 0.4943^\circ$$
$$\theta_{min2} = 1.0956^\circ$$
$$\theta_{min3} = 1.6458^\circ$$
$$\theta_{min4} = 2.3599^\circ$$

$\Delta\theta$ was then averaged out for the different measurements, and hence a value of the thickness Δ was obtained from Equation 19 to be $\Delta = 31.74$ Å.

These measurements were repeated for different scans. Table 1 tracks the changes on the thickness for different temperatures and different times, considering some selected scans.

Scan Number	**Temperature**	θ_{min}	Δ **(Å)**
172	Room temperature	0.4943 1.0956 1.6458 2.3599	31.74
313	Room temperature	0.3983 0.8397 1.3963 1.8505 2.4391	38.69
348	164 °C	0.3983 0.8013 1.2428	46.75
384	290°C	0.2788 0.5364	76.62
444	340°C	0.2788 0.5000	89.23

Table 1: **Different measurements of the thickness of the film**

It is clear that the reflectivity scans are affected by time and temperature. The longer we wait, and the higher the temperature, the greater the thickness of the film is. This is not related to an increase in the gold layer, since no more gold was deposited. Figure 10 shows the different plots for the reflectivity analysed in Table 1. As we can see, the oscillations become fainter and fainter as the temperature increase, and as a consequence it is also harder to obtain a good value for the minima.

The measurement selected for this analysis were, in my opinion, the ones that best show the changes on the sample. Further measurements were obtained on the sample after cooling down, but these do not show any oscillations. Also, we have to remember that after four days more gold was deposited on the sample. Similar reflectivity measurements were taken in

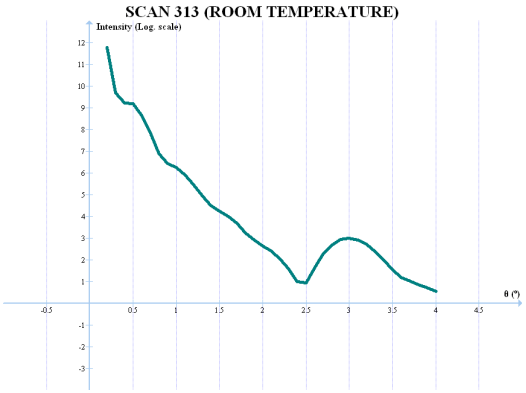

(a) Scan 313 at Room T

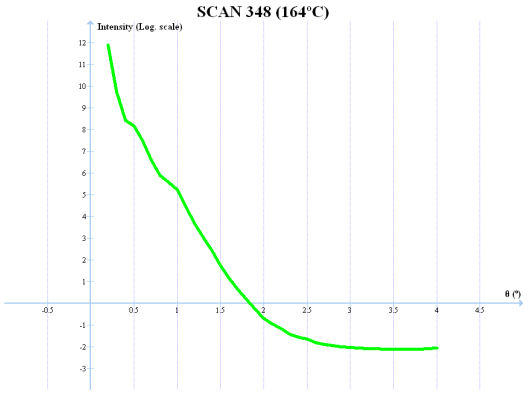

(b) Scan 348 at 164°C

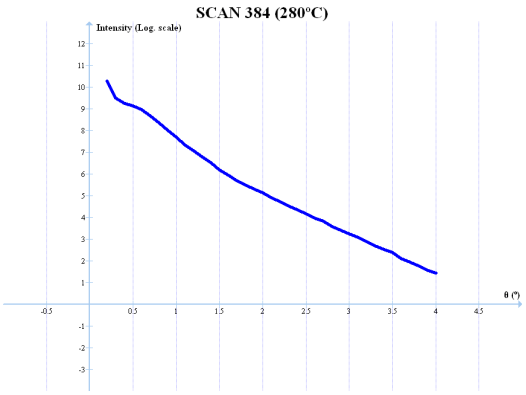

(c) Scan 384 at 290°C

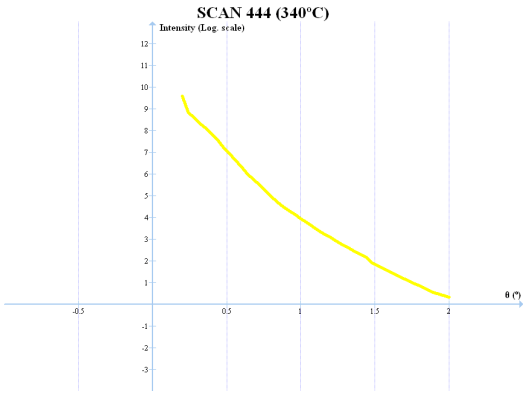

(d) Scan 444 at 340°C

Figure 10: **Different scans of the reflectivity**

this new condition, and the results obtained at room temperature was $\Delta =$ 68.9 Å.

3.3 Error analysis

The uncertainty on the thickness was estimated starting from the valuation of the error on obtaining the proper value for the diffraction angle at the minima of the periodic oscillations. This error was estimated to be

$\mathrm{d}\theta = 0.005°$ for the scans with T $\leq$ 200°C and
$\mathrm{d}\theta = 0.01°$ for the scans with T $\geq$ 200°C.

This estimate increases due to the fact that the oscillations are less clear for higher temperatures. Then the minimum and the maximum values for the thickness are given by Equation 20 and 21 respectively:

$$\Delta_{min} = \frac{\lambda}{2\sin(\Delta\theta + \sqrt{2}d\theta)} \tag{20}$$

$$\Delta_{max} = \frac{\lambda}{2\sin(\Delta\theta - \sqrt{2}d\theta)} \tag{21}$$

Here $\Delta\theta$ indicated the average value for the width of the oscillations in terms of θ, and to this value for the angle the combined error for two measurements (i.e. $\sqrt{2}\mathrm{d}\theta$) is either added or subtracted, according on what type of measurement is aimed to achieve.

Scan	Δ **(Å)**	Δ_{min} **(Å)**	Δ_{max} **(Å)**	**Abs error (Å)**	% **error**
172	31.74	32.11	31.38	0.36	1.14
313	38.69	39.23	38.16	0.54	1.39
348	46.75	47.54	45.98	0.78	1.68
384	76.62	81.06	72.64	4.22	5.51
444	89.23	95.33	83.87	5.73	6.42

Table 2: **Errors on the thickness of the film**

Table 2 shows the minimum and the maximum value to the reflectivity for each one of the measurement assessed here, together with an estimate

of the percentage error, obtained by calculating the difference minimum and the maximum value and dividing it by two to find an average absolute error.

The error increases from being around 1% to 6.4% as the sample goes towards its melting point.

4 Crystal Truncation Rods

4.1 Introduction to CTR

Crystal Truncation Rods are one of the most powerful tools for analysis of the surface structure since their discovery.

When an x-ray beam diffracts from a theoretical 2D plane, its intensity is given by a 1D rod perpendicular to this plane in reciprocal space. This plane can also be seen as a surface, and when a bulk crystal is added to this 2D picture, we will also obtain sites of maximum intensity at the Bragg peaks, allowed by selection rules determined by the type of crystal analysed.

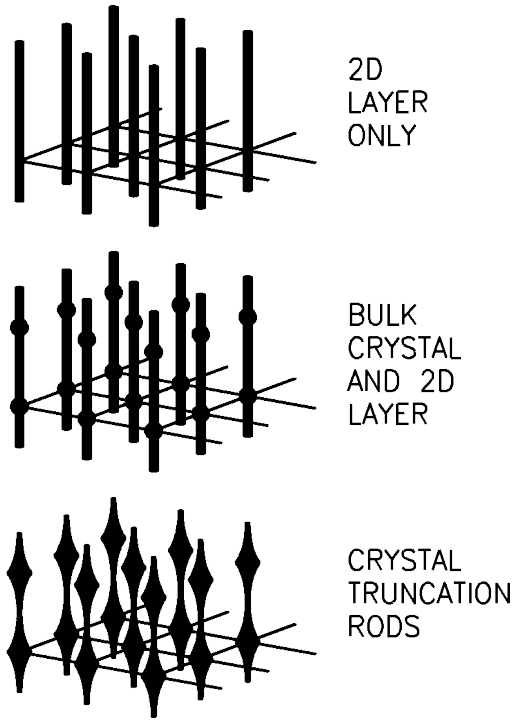

Figure 11: **Observations of a CTR** - This schematic figure shows how a 2D surface with the addition of a bulk crystal gives rise to a pattern in the intensity along the rod created by diffraction from the surface

.

Contribution from both the surface and the bulk is what is measured in a CTR scan, and it is therefore what allows us to obtain a model for the

structure of the surface. A scheme of these different steps taken to define the CTRs is shown in Figure 11. The rod originates from adding up all the crystalline layers, which are brutally cut down in the presence of a definite surface. Note that gold evaporated on top of the silicon is not a crystal, it is a powder, hence what we will measure as CTR scans in the experiment is the physics and the structure at the interface. The goal is to find a good fit of the data by finding a plausible structure factor which agrees with the measurements. The modulus square of the structure factor has to agree with the observations, i.e. the intensity of the CTR measured, as described in Equation 14. The starting point is to consider the different contribution of the (semi) infinite crystalline layer to obey Equation 22:

$$A_{CTR}(L) = \sum_{n=1}^{\infty} e^{iLa_0 n} = \frac{1}{1 - e^{iLa_0}} \tag{22}$$

Equation 22 was obtained from the definition of the structure factor (Equation 12) and Laue condition (Equation 8) using some simple algebra and trigonometric identities and the simple relation between Q and L (see Equation 11).

Here the amplitude coming from the CTR is given in terms of the Miller index L in units of 2π and the silicon lattice constant a_0. The only thing accounted for in this equation is the amplitude of a scattered wave due to the presence of a crystal with a truncated layer (i.e. the surface). Equation 22 has to be multiplied by the structure factor of silicon in order to give a good approximate of a fit. To this result, a gold contribution has to be added in order to find a final model.

Silicon is a diamond crystal and has therefore a face-centered cubic unit cell with four extra atoms at $(\frac{1}{4}\frac{1}{4}\frac{1}{4})$, $(\frac{1}{4}\frac{3}{4}\frac{3}{4})$, $(\frac{3}{4}\frac{1}{4}\frac{3}{4})$ and $(\frac{3}{4}\frac{3}{4}\frac{1}{4})$. There are many ways of accounting for the unit cell of this crystal. We can think of it as a simple diamond lattice with gold vaporised on top, using the usual Miller indices notation to work it, or simplify everything by defining a new unit cell, as shown in Figure 12(a).

In our experiment, measurements were made along the 11L rod. Defining the unit cell according to our needs, we can consider the scans to be made along the 10L rod. The measurements identified with this new unit cell are taken in surface units, as compared to bulk units, the usual way of defining a diamond lattice unit cell. This way is more useful for our purposes, since

considering a simpler unit cell with fewer atoms in it is easier to manage than the usual diamond one.

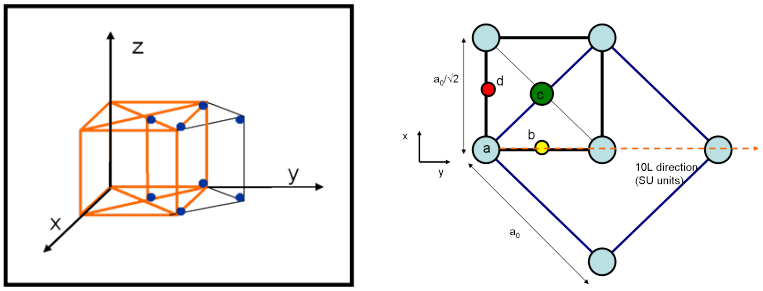

(a) 3D (b) 2D from top

Figure 12: **(a) Defining a new unit cell in 3D** - This figure shows the two different definitions of a unit cell. The orange cube indicates the usual diamond one (lattice points have been left out); the unit cell used in most of our analysis is the one defined by the blue lattice points, which is simpler and smaller. The unit cell lattice constant now is not the same for all (x, y, z) directions: it changes in length from the standard silicon one in all but the z direction, to $\frac{a_{Si}}{\sqrt{2}}$. **(b) Diamond unit cell in surface and bulk units in 2D** - This sketch represents the diamond unit cell as seen from above. The black square indicates surface unit cell, while the dark blue one shows the conventional one. Each circle indicates a silicon atom, and the different colour represent different heights within a unit cell in a spiral-like way proper for a diamond crystal. The lattice sites labelled a, b, c and d are where the gold atoms may be positioned in the different models. The red and the yellow atoms indicate two of the four atoms which differ a FCC crystal and a diamond one. The green atom is the 'face' in the lower layer (at $\frac{a_0}{2}$). The dashed orange arrow indicates how the 11L rod becomes 10L in surface units.

For more information on this technique, see reference [3].

4.2 Observations

4.2.1 Gold powder rings

As discussed in Section 4.1, the CTR scans were measured along the 10L rod in surface units: let's not forget that this is analogous to the 11L rod in bulk units, hence, being silicon a diamond crystal, due to the selection rules discussed in the Introduction, only the 101 and 103 Bragg peaks are allowed for such crystal in such units. Most of the scans were taken for $0.15 \leq L \leq 2.99$. Take for example Figure 13: this scan was taken on the frozen sample, after having been heated up once already above T_E. As we can

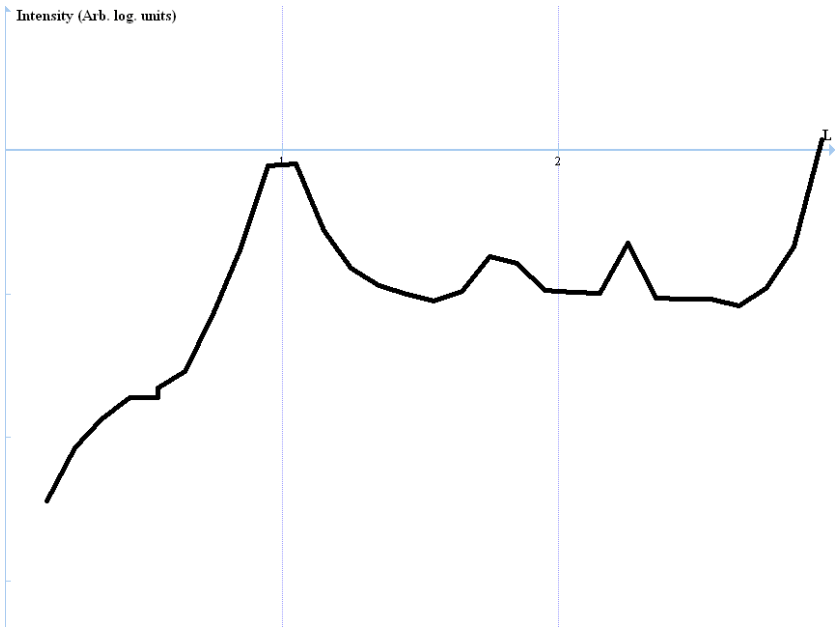

Figure 13: **Scan on cold sample** - This CTR scan clearly show the presence of two Bragg peaks at L = 1 and L = 3. The presence of two other small peaks was though not predicted, but explained to originate from the presence of powder rings gold 111 and 200 peaks.

.

see, the presence of two other peaks was detected at L = 1.82 and L = 2.27. These are caused by an additional contribution from powder diffraction of the vaporised gold on top. Powder diffraction originates from the fact that gold is not crystalline in this experiment, but it is a powder of atoms randomly deposited on the silicon surface. A sketch of the powder rings geometry is shown in Figure 14(a) and 14(b). The FCC nature of gold should allow for Bragg peaks at 111 and 200, and in the next few lines I will prove that what we observe is actually due to these two peaks. This is easier if worked out in bulk units (i.e. considering the scans as along the 11L peak).

It is simple to deduct these results starting from Laue condition for constructive interference, defined in Equation 8 in the Introduction. This result is equivalent to Bragg's law (Equation 1) but more precise. According to Laue's condition, the distance d between the planes for a cubic crystal is closely related to the lattice constant of a material a_0, as shown below:

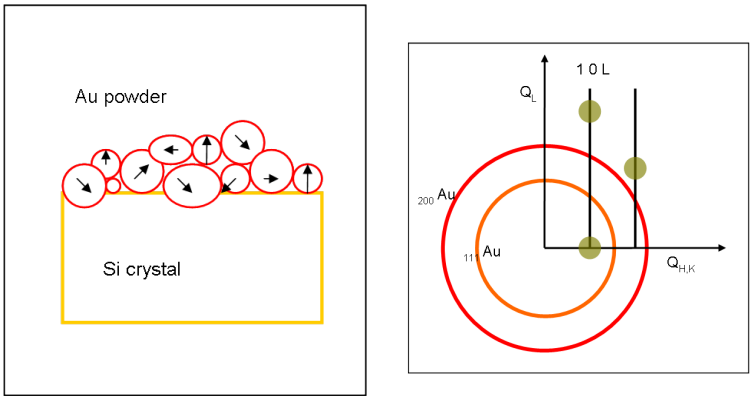

(a) (b)

Figure 14: **Powder rings geometry** - Figure (a) is a (out of scale) sketch of the silicon sample with randomly orientated gold on top; Figure (b) is a schematic representation in reciprocal space of the CTR scan, showing the 10L rod and how the 111 and the 200 powder rings contribute to its intensity.

$$d = \frac{a_0}{\sqrt{H^2 + K^2 + L^2}} \tag{23}$$

By combining this equation with Bragg's law and the definition of the momentum transfer (see Equation 4), we can obtain an expression for the gold momentum transfer:

$$Q_{Au} = 2\pi \frac{\sqrt{(H^2 + K^2 + L^2)_{Au}}}{a_{Au}} \tag{24}$$

What we are looking for here is the (HKL) of the extra gold peaks. To do so, we have to obtain the a value of momentum transfer Q from the plots using the silicon Miller indices at the extra peaks (i.e. in bulk units $(HKL)_{Si}$ = (1 1 1.82) and (1 1 2.27)). Hence

$$Q_{Si} = 2\pi \frac{\sqrt{(H^2 + K^2 + L^2)_{Si}}}{a_{Si}} \tag{25}$$

Note that the value of $\sqrt{(H^2 + K^2 + L^2)}$ is different for Equations 24 and 25, the first one is related to the gold peaks and the second one is the

silicon one. Equating the two momentum transfers in 24 and 25 we obtain an expression for the Miller indices of the gold Bragg peaks, which is what we are looking for:

$$\sqrt{(H^2+K^2+L^2)_{Au}} = \frac{a_{Au}}{a_{Si}}\sqrt{(H^2+K^2+L^2)_{Si}} \tag{26}$$

Now, the lattice constants for gold and silicon are, respectively:
$a_{Au} = 4.080$ Å
$a_{Si} = 5.431$ Å

Therefore, simply putting in these values and using $L_{Si} = 1.82$ and 2.27 we obtain:

$$\sqrt{(H^2+K^2+L^2)_{Au}} = 1.732 \approx \sqrt{(1^2+1^2+1^2)} \tag{27}$$

and

$$\sqrt{(H^2+K^2+L^2)_{Au}} = 2.009 \approx \sqrt{(2^2+0^2+0^2)} \tag{28}$$

These values clearly show that these two peaks are the 111 and 200 gold Bragg peaks. As the temperature increase, and the sample melts, these peaks are seen to disappear, as it is expected since they are a signature of the solid state of the gold in the sample. They reappear again when the sample is frozen once again.

4.2.2 Roughness

The roughness of the surface of sample can be tracked by monitoring how the intensity in between the L = 1 and L = 3 peaks change. The expectation is that the roughness of the sample increases as the time goes on, as the sample is being manipulated more and more. Also, it is reasonable to think that when the temperature is high, the roughness is also higher.

The increase in the roughness is shown in the scans as a deviation from the theoretical CTR shape represented by a decrease in the intensity in between the peaks. Equation 22 assumes a contribution from a perfectly smooth surface, as a semi-infinite crystal, starting the sum from n = 1 to ∞. If we include a rough surface (see Figure 15(a)), sum in Equation 22 becomes

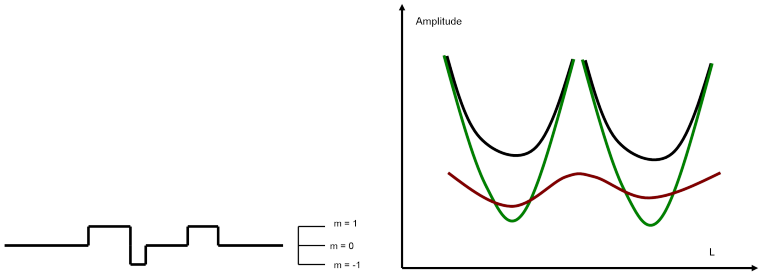

(a) A sketch of a rough surface (b) CTR change in the presence of roughness

Figure 15: **Sketches of a rough surface (a) and a model for a CTR scan in the presence of roughness (b)** - In (a) the parameter m is an integer indicating how much does the surface deviates from the ground level m = 0. The misalignments are in steps of one ML. Figure (b) shows a theoretical CTR scan on a smooth surface (black line); roughness is then accounted as a cosine-like contribution (bordeaux line); when the two are added together the result is the green line, representing a CTR scan on a rough surface.

$$A_{rough} = \sum_{m}^{\infty} e^{iLa_0 n} = \frac{e^{iLa_0 m}}{1 - e^{iLa_0}} = \frac{\left(P(0)e^{iLa_0 0} + P(+1)e^{iLa_0 1} + P(-1)e^{iLa_0(-1)} \ldots\right)}{1 - e^{iLa}} \tag{29}$$

The term m = 0 defines the 'sea level' of the surface (see Figure 15(a)), the starting point. The roughness creates the deviation in m. P(m) is the probability of a surface being at level m. This whole contribution gives rise to a cosine wave, and considering the Bragg peaks to be in units of 2π, this cosine-like wave will give rise to destructive interference at L = π, i.e. in between the Bragg peaks. This is why the intensity in the middle decreases as roughness increases (see Figure 15(b)).

Figure 16 shows some measurements taken at different times and temperatures, and we can clearly see that the intensity in between the silicon Bragg peaks changes with temperature and time. If we then assume that the roughness is proportional to how intense is the trough, we can infer that the sample at the beginning is quite smooth. Then as we increase the temperature the roughness of the surface also increases, maximising for T = 450°C. On cooling down the surface becomes smoother, but not as quite as at the beginning.

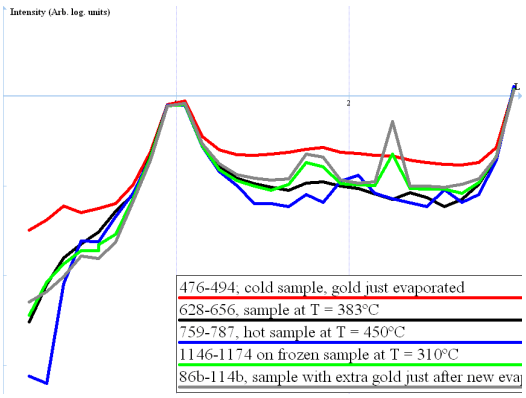

Figure 16: **Different CTR scans to show the reflectivity** - This figure shows four CTR scans taken at different temperatures. The red scan was taken on the cold sample just after the first evaporation, the black one was taken on the melted sample, the blue one on the very hot sample and finally the green one on the solid sample after freezing. The gray scan shows how the intensity changes on the cold sample just after the second deposition.

When more gold was evaporated on the sample, the roughness does not really improve much. If this extra gold was evaporated in such a way that it can be considered as just sitting above the old one (as it should be if the gold was deposited uniformally), it would reproduce the position of the previous surface at every point and hence it should not change the roughness.

4.3 Calculations for fits

The greatest achievement of studying CTRs is the acquirement of a good model for the surface structure, or in our case for the structure of the interface. I tried to do this manually for different model, starting from the simplest case (a fit for a simple cubic silicon, which was never expected to match, but it was a start) in order to reach (in steps) a more complicated one, considering the silicon diamond lattice and the presence of gold. The fits were compared with a scan on cold sample with just evaporated gold assuming no roughness, and all the parameters were adjusted in order to fit this model. Successively, in order to improve the quality of my fits, I used the ANAROD package, which is a computer program studied for the purpose of finding a model of CTR scans.

4.3.1 Manual fits

The purpose was now to use the definition of the structure factor (see Equation 22) to fit the scans. The detector measures the intensity of the outgoing wave, which is closely related to the structure factor according to Equation 14. Hence, for the first fit we assumed the simplest relation between the two, i.e.

$$I(Q) = |F(Q)|^2 \tag{30}$$

Hence combining Equation 22 with Equation 30 the following model for the intensity was obtained:

$$I(L) = \frac{f_{Si}^2}{4\sin^2(\pi L)} \tag{31}$$

This fit is shown in Figure 17.

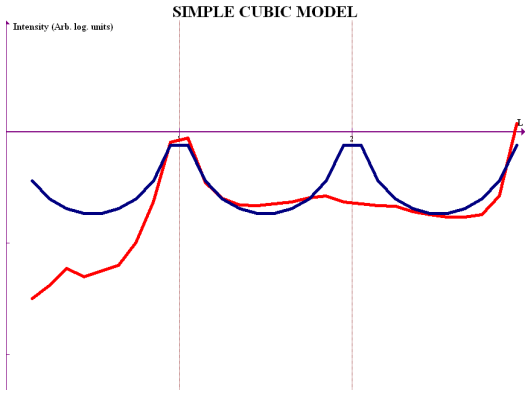

Figure 17: **Simple cubic fit on CTR** - This figure shows the fit as if our sample was only made up by a simple cubic lattice (blue scan), as compared with observations on the cold sample (red scan). This model clearly does not fit but it is a good place to start in order to build a better one.

Clearly, one can see an extra peak in the model at L = 2, which is not observed in the silicon diamond lattice since it is forbidden by selection rules. Also, for L smaller than 1 the fit does not agree at all with the data. The next step is therefore to account for a FCC crystal lattice, which is a step closer to the diamond lattice we know the silicon to be. The structure factor

of a FCC is given in the Introduction by Equation 15. If we include the known values of H and K in this expression (i.e. H = 1 and K = 1 in bulk units) we obtain a simple expression of the structure factor of a (11L) FCC crystal in terms of L:

$$F_{FCC}(L) = 2f_{Si}(1 - e^{i\pi L}) \tag{32}$$

Squaring the modulus of Equation 32 we obtain the intensity of a FCC model for the given values of the Miller indices

$$I_{FCC}(L) = |F_{FCC}(L)|^2 = 16f_{Si}^2 \sin^2 \frac{\pi L}{2} \tag{33}$$

We can now combine Equation 22 and Equation 32 in order to obtain a model for an FCC sample. Multiplying the two, we get:

$$F_{FCC}^{Si}(L) = f_{Si}\frac{2(1 - e^{i\pi L})}{1 - e^{i2\pi L}} \tag{34}$$

Hence, taking the modulus square of Equation 34 we finally get the intensity for a FCC silicon sample:

$$I_{FCC}^{Si} = \left|F_{FCC}^{Si}\right|^2 = \frac{4f_{Si}^2 \sin^2 \frac{\pi L}{2}}{\sin^2(\pi L)} \tag{35}$$

This expression gives the fit shown in Figure 18. The ghost Bragg peak at L = 2 disappeared. The fit is though still very bad in between the two main peaks, the reason being that no gold was yet considered.

In order to create a model which account for gold, the best way is to add to the FCC structure factor the structure factor of gold, i.e.:

$$F_{FCC}^{Tot}(L) = F_{FCC}^{Si}(L) + F_{Au}(L) \tag{36}$$

Substituting Equation 34 in Equation 36 and taking $\mathrm{F}_{Au} = \mathrm{f}_{Au}\mathrm{e}^{i2\pi Lz}$, the total structure factor for FCC becomes:

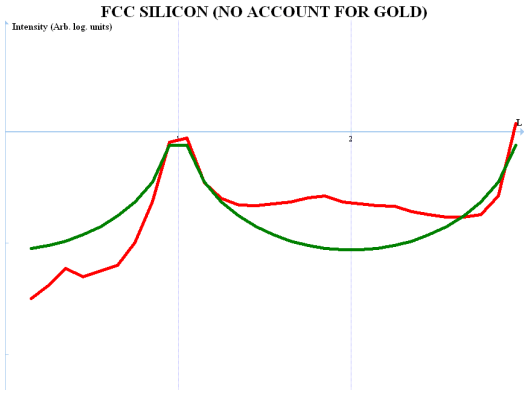

Figure 18: **Silicon FCC fit on CTR** - Here we show the fit of CTR scans accounting for the sample to be a face centered cubic silicon crystal (green scan), as compared with a scan on cold sample (red scan). This model is improving, although still very imperfect.

$$F_{FCC}^{Tot}(L) = f_{Si}\frac{2(1-e^{i\pi L})}{1-e^{i2\pi L}} + f_{Au}e^{i2\pi Lz} \tag{37}$$

The parameter z is a dimensionless quantity which indicates the distance between the last silicon atom in the bulk and the first gold atom in the surface in terms of a_0^{Si}. The unknowns to be manipulated to improve the fit in this case are z, f_{Si} and f_{Au}, the two atomic form factors. In this case, the ratio atomic form factors indicate the occupancy of the interface, i.e. how much gold is there with respect to silicon.

If we convert Equation 37 into intensity we obtain:

$$I_{FCC}^{Tot}(L) = 4f_{Si}^2\frac{\sin^2(\frac{\pi L}{2})}{\sin^2(\pi L)} + f_{Au}^2 + 4f_{Si}f_{Au}\frac{\sin(\frac{\pi L}{2})}{\sin(\pi L)}\cos(2\pi Lz) \tag{38}$$

Figure 19 shows the best fit for this model, obtained considering z = 0.55, $f_{Si} = 1.2$ and $f_{Au} = 1.1$.

The fact that the form factors are similar in size does not mean that the amount of Si and Au at the interface is equal. The form factors account for the electron density, and they are usually approximated to be equal to the atomic number Z. In this case, $Z_{Au} = 79$ and $Z_{Si} = 14$. Hence for a total occupation of gold at the interface, we should consider f_{Au} to be around 5.6 times greater than f_{Si} for a first layer with 100% gold. So we can infer from

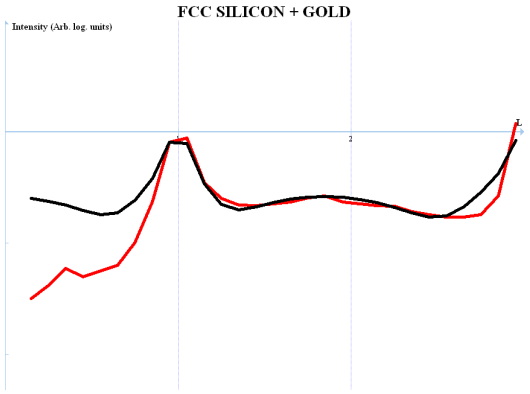

Figure 19: **Silicon FCC + Gold fit on CTR** - This model (black line) accounts for the presence of gold in the sample and we can clearly see an improvement. The fit is still not perfect though, so the next step is to account for the bulk diamond crystal lattice.

these measurements that the interface is somehow a mixed layer between gold and silicon. f_{Si} in this case acts a scale factor which allows to normalise the fits to get good agreement at the Bragg peaks.

So far we have ignored the fact that the silicon crystal has a diamond structure and therefore, together with the fcc unit cell there are additional four atoms at $(\frac{1}{4}\frac{1}{4}\frac{1}{4})$, $(\frac{1}{4}\frac{3}{4}\frac{3}{4})$, $(\frac{3}{4}\frac{1}{4}\frac{3}{4})$, $(\frac{3}{4}\frac{3}{4}\frac{1}{4})$. Therefore there the gold could sit on top of any one of the extra four atoms, and not necessarily on one of the main FCC lattice sites. The basis has now changed, hence the structure factor of silicon becomes:

$$F_{Diam}^{Si} = f_{Si}(1 + e^{2i\pi(\frac{1}{4}H+\frac{1}{4}K)})(1 + e^{2i\pi L}) \tag{39}$$

As before, we are analysing the 1 1 L rod (in bulk units) so H and K both equal 1. Therefore the first bracket in Equation 39 becomes only (1 + i). Hence, this term simply becomes a phase shift that accounts for the possibility that gold may lie on top of the extra atoms. So the total structure factor becomes:

$$F_{Diam}^{Tot} = (1 + i)\left[2\frac{f_{Si}(1 - e^{i\pi L})}{1 - e^{i2\pi L}} + \frac{f_{Au}}{\sqrt{2}}e^{-i\frac{\pi}{4}}e^{i2\pi Lz}\right] \tag{40}$$

And the scattered intensity is hence:

$$I_{Diam}^{Tot} = \left\{ 4f_{Si}^2 \frac{sin^2(\frac{\pi L}{2})}{sin^2(\pi L)} + f_{Au}^2 + 4\sqrt{2} f_{Si} f_{Au} \frac{\sin(\frac{\pi L}{2})}{\sin(\pi L)} \cos\left((2Lz - \frac{1}{4} + \frac{L}{2})\pi \right) \right\} \tag{41}$$

Equation 41 gives us the final (manual) model, which is represented in Figure 20.

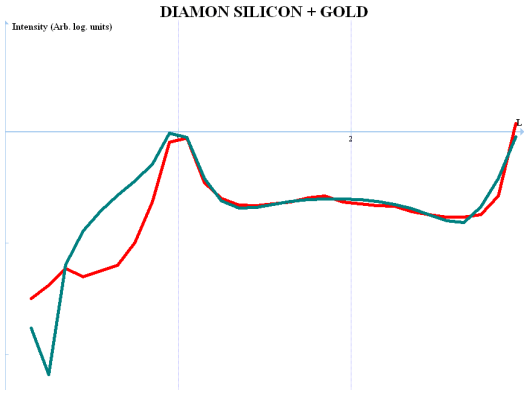

Figure 20: **Final manual fit on CTR** - The blue line shows the final model which takes into account a silicon diamond bulk, together with the thin gold films. It is here compared with a sample observation CTR made on the cold sample (red line). The fit does not quite agree with the observation, but it is the best one so far.

The parameters which have been manipulated are the same as before, and the best fit was found for z = 0.33, f_{Si} = 1 and f_{Au} = -0.7. These parameters differ strongly from the ones previously used, especially the form factor of gold which is negative in this case. A negative gold form factor gives a negative occupancy. This parameter is simply a fraction of how much gold is present in the first layer above silicon: hence a negative occupancy is unphysical. What this means is that the gold does not sit exactly on top of the silicon for this Although the agreement between this model and the observations is good in between the Bragg peaks, it is clear from the picture that this fit is not yet perfect. The model suggests only an expected asymmetry between the left and the right of the L = 1 peak, but the precise features are not defined. This is why we decided to turn to ANAROD, a computer program studied for the purpose of fitting CTR scans.

4.3.2 Fits with ANAROD

The package ANAROD is able to reads different files and to differentiate them. Each file contains different information. It first reads a bulk file, which for our purposes consists of four silicon atoms at four different lattice sites. This is shown in Figure 12(b), where the positions a, b, c and d indicate the four different sites on top of which a gold atom can sit. Secondly, a surface file containing the position of one or two (according to the model) gold atoms must also be inserted. These two files define the unit cell (in surface units, as defined in Figure 12(b)), and hence a theoretical calculation of the 10L rod can be done.

This CTR is then combined with a data file containing the observation, i.e. the measured amplitude. The data file were exctracted by Newplot, a program used throughout the experiment in order to manipulate the plots obtained. Newplot though provides a value for the intensity of the observation. Hence using Equation 14 the structure factor was obtained. The data file also has to account for an error on the structure factor. This was assumed to be 5 % of the structure factor itself throughout the whole rod but at the positions closest to the Bragg peak, for which the error was increased to 10 %. In order to improve the fit some parameters can be changed: the scale factor, the displacement and the occupancy. The first one works as a normalisation factor. The second and the third one account respectively for the distance between the first gold atom and the last silicon atom, in units of a_{Si} (the parameter we previously called z), and for the relative amount of gold and silicon (previously considered as the ratio between f_{Au} and f_{Si}).

Two main models were proposed, one having only one atom in the surface file, and the other one containing two, at different heights. All the possible combinations were analysed (aa, ab, ac... and so on, as defined in Figure 12(b)) and for both the 1- and the 2-atoms models many combination were shown to be equivalent, giving the same value for X^2 and using the same fitted parameters. These analogies are explained from the fact that for some cases the positions of the atoms of the different combinations turn out to be identical. The different parameters obtained for different models and the corresponding values of the X^2 are shown in Table 3.

This Table clearly shows that many of the models are the equivalent. Moreover, the X^2 is enormously high for all the models.

This shows that the fits are not very good, and this is material for further

Lattice site	X^2	Scale factor	Displacement	Occupancy
a	44.4268	0.0664	1.2704	0.0368
b	28.0679	0.0614	0.0423	0.0705
c	28.0679	0.0614	0.0423	0.0705
d	44.4268	0.0664	1.2704	0.0368
aa	46.4670	0.0657	1.2974	0.0188
ab	39.6013	0.04635	-0.02316	0.2469
ac	39.6013	0.04635	-0.02316	0.2469
ad	74.5842	0.0595	0.4584	0.0457
ba	43.7185	0.0424	0.0236	0.1161
bb	44.6308	0.0675	0.4771	0.0316
bc	44.6308	0.0675	0.4771	0.0316
bd	43.7185	0.0424	0.0236	0.1161
ca	43.7185	0.0424	0.0236	0.1161
cb	44.6308	0.0675	0.4771	0.0316
cc	44.6308	0.0675	0.4771	0.0316
cd	43.7185	0.0424	0.0236	0.1161
da	74.5842	0.0595	0.4584	0.0457
db	39.6013	0.04635	-0.02316	0.2469
dc	39.6013	0.04635	-0.02316	0.2469
dd	58.8757	0.0627	1.6702	0.0279

Table 3: **X^2 and parameter values for different models**

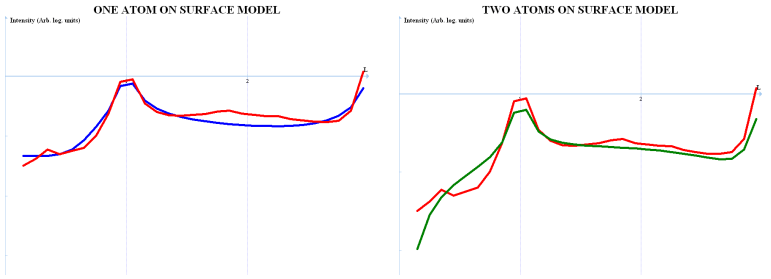

(a) Model with one gold atom on the surface, at position b, analogous to c

(b) Model with two gold atoms on the surface, at position ac, equivalent to ab, db and dc

Figure 21: **ANAROD fits for two different models**

studies which will be carried out in the next few months. Figure 21(a) and 21(b) show the two best fits obtained with the 1-atom and 2-atoms surface models respectively.

We can see that the best fit is the left one in Figure 21(a), but it is still not perfect. In between the two peaks the model does not account perfectly for the presence of gold, which causes the bump in the middle. Hence more work should be done.

5 Grazing Incident Diffraction

5.1 Background information

Grazing Incidence X-ray Diffraction is a technique which aims to analyse only the last few monolayers of a sample. A beam of x-rays is shone on the sample at a very low incident angle (μ in our set up); this angle is chosen to be smaller than the critical angle α_C. This then gives total internal reflection and hence the only information we are given is a contribution from the surface. An evanescent wave propagates through the substrate, and this will penetrate only for few layers since its intensity will decay exponentially, so this is why it is used to study the last few monolayers of a sample. In the experiment GID was used to track the changes on the state of the surface, and the aim was to check and try to reproduce Oleg Shpyrko's results of a crystalline surface layer above the eutectic temperature.

The peaks we expected to observe were of four different kinds. First, a crystalline silicon contribution could be seen as broad peaks which originate from the detection of particular bulk silicon Bragg peaks. This is shown in Figure 22, and since we do not want to observe these contributions, it is just a matter to choose a convenient direction in reciprocal space in order to avoid them.

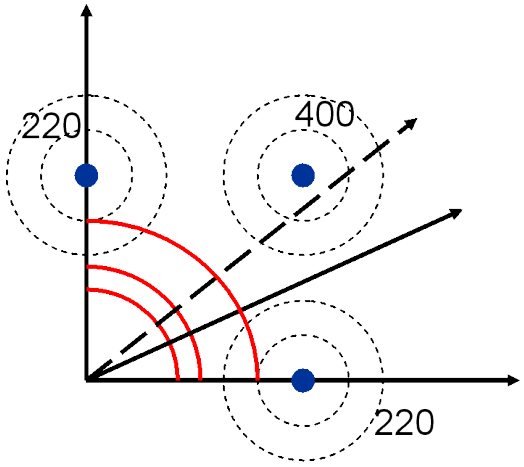

Figure 22: **Sketch indicating the need to avoid unnecessary contribution to the GID scan from silicon Bragg peaks in reciprocal space.**

Secondly, another contribution from crystalline 111 and 200 gold is ex-

pected on the solid sample below the eutectic temperature as sharp intense peaks seen at an angles governed by Bragg's law, analogous to the ones studied for the CTR in Section 4.2.1. These peaks should disappear as the sample melts at the interface, and a broad liquid peak should take its place. This is the hallmark of a liquid sample, and is caused by short-range ordering of the gold-silicon atoms in the liquid form. Together with all the above, crystalline surface peaks should also be seen. These are expected to be there on the frozen sample, but the crystalline layer on the surface observed by Shpyrko will be confirmed if and only if these peaks are shown to be present on the liquid sample (i.e. together with the broad liquid peak).

For more information on the GID technique, refer to [6].

5.2 Results

More than one hundred GID scans were taken in the experiment: the ones showed in this section are simply the most representative of the changes in the sample. Figure 23 shows five of the most exemplary scans as a sequence.

One of the most important tasks of this project was to analyse the different scans shown in Figure 23 and compare the angles of the peaks with the ones obtained by Shpyrko and discussed in Section 1.3. Figure 23(a) is a scan of the GID intensity in log scale against the angle 2θ on the frozen sample. The two very intense sharp peaks are contributions from the gold powder rings and represent the 111 and the 200 Bragg peaks present on FCC gold. Together with these features though, we can clearly see some other smaller sharp peaks: these peaks come from the crystallinity of the surface. This is not surprising, since the sample is frozen, there is no reason for which these should not be seen.

The second scan, seen in Figure 23(b), represents the sample at 385°C. On heating up, we were very careful on tracking the temperature, it was increased slowly in steps of around 3°C, and we started to observe a full broad liquid peak only at this temperature. This peak is the hallmark of a liquid metal, and its presence was therefore assumed to be the evidence of the liquid state of the interface. Figure 23(b) is one of the most important scans of the experiment since it indicates the presence of surface Bragg peaks together with the broad liquid peak. This shows that there is at least one crystalline layer at the very surface of the sample above the eutectic temperature and it therefore confirms the observations of Oleg Shpyrko.

He also observed evidence for a solid-solid surface phase shift on the sam-

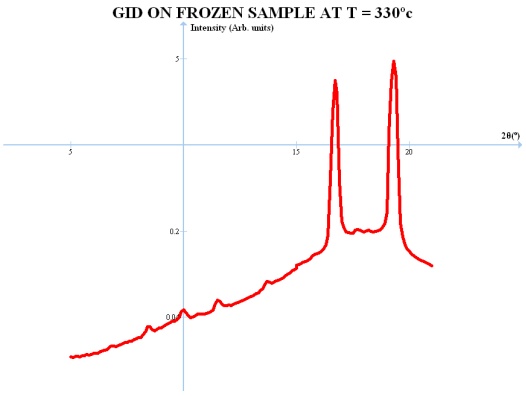

(a) GID on frozen sample at T=330°C

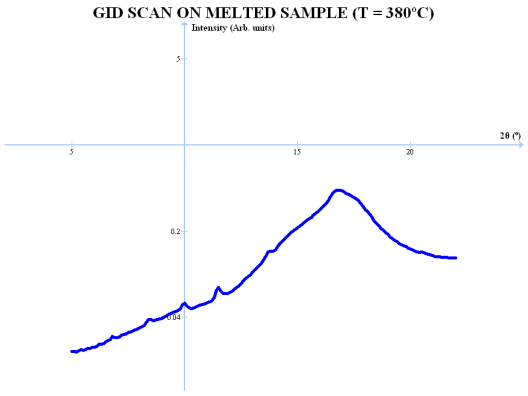

(b) GID on melted sample at T=385°C

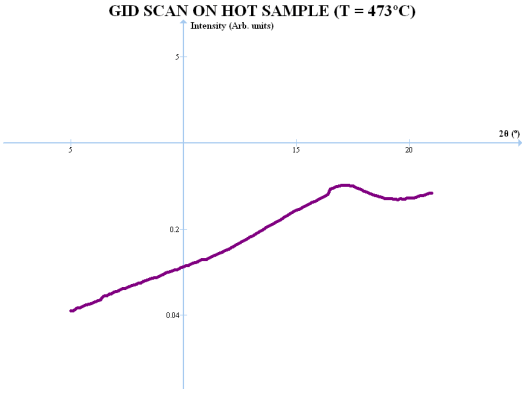

(c) GID on very hot sample at T=473°C

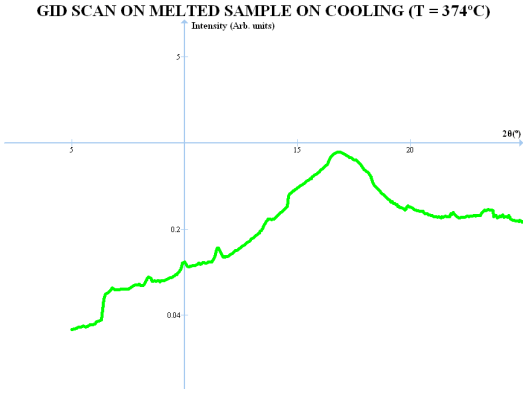

(d) GID on melted sample on cooling at T=374°C

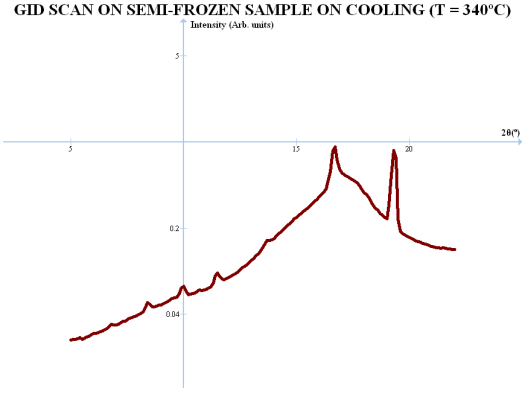

(e) GID on semi-frozen sample on cooling at T=340°C

Figure 23: Different GID scans at various temperatures

ple, and the complete disappearence of the peaks at around 430°C. Figure 23(c) shows a GID scan at a very high temperature (473°C), a very broad liquid peak is seen and no more evidence for the crystalline layer on the surface is observed, as expected. The liquid peak is seen to be somehow broader at this very high temperature: this feature was not analysed but it will be material for further studies on the sample. Our measurements did not account for any shift in the peaks, hence no phase transition was observed, in contrast with O. Shpyrko's result.

Figure 23(d) is a very neat scan taken at 374°C on cooling down the sample. As we can see the AuSi interface is still liquid, but the presence of the peaks is once again confirmed. This shows that the crystallisation of the surface is a very riproducible feature.

Finally, Figure 23(e) shows the sample at 340°C in a semi-frozen state: this means that both powder ring sharp peaks (hallmark of the solidity of the sample) and the liquid peak (signature of the presence of a liquid) are present. Hence the sample is observed here to freeze, at a temperature 40°C lower than its melting point. This is evidence for some sort of supercooling.

The next step was is to compare the angle observed in the experiment with the ones obtained by Shpyrko. Figure 4, in the Introduction, shows the plot of Intensity against momentum transfer Q obtained by O. Shpyrko. From this plot, the valued of the momentum transfer at the peaks was extrapolated, and converted in units 2θ to compare it with out scans. This conversion was simply done by using the definition of the momentum transfer given in Equation 4, taking the wavelength of our experiment's x-ray ($\lambda = 0.689$Å) beam to allow comparison. This becomes:

$$2\theta = 2 \arcsin\left(\frac{Q\lambda}{4\pi}\right) \tag{42}$$

The program Newplot was then used to fit each peak related to the crystalline surface in order to obtain a value of 2θ for the maxima. The FWHM was also noted down for error calculations (see next Section). Table 4 shows the diffraction angle and momentum transfer comparison between our measurements and Shpyrko's ones.

It is clearly seen that the measurements agree quite well, although some of them are not perfect. In particular, one of the peaks Shpyrko observes was not observed in our scans, maybe obscured by the very intense powder ring

$\mathbf{Q}_{Shpyrko}$ (Å)	$\mathbf{2\theta}_{Shpyrko}$ (°)	$\mathbf{2\theta}_{Exp}$(°)	$\mathbf{Q}_{Exp}$ (Å)
1.075	6.76	6.78	1.078
1.333	8.38	8.41	1.337
1.575	9.91	9.96	1.583
1.683	10.59	10.61	1.686
1.817	11.44	11.47	1.823
2.150	13.54	13.66	2.169
2.592	16.34	X	X
2.650	16.71	16.71	2.650
2.783	17.55	17.65	2.798
2.842	17.93	18.18	2.881
X	X	19.30	3.057
3.133	19.78	19.95	3.159
3.217	20.32	20.53	3.250
3.367	21.28	21.27	3.366
3.433	21.70	21.89	3.463
3.658	23.14	23.43	3.703
3.967	25.13	24.36	3.848

Table 4: **Comparison between experimentally observed surface crystalline peaks and the ones observed by O. Shpyrko**

peak at 16.71°. Moreover, Shpyrko did not find any evidence for the peaks we observed at $2\theta = 19.30°$. However, the 19.30° peak corresponds to the 200 powder Bragg peak: using the same technique (see Equation 43) used in Section 4.2.1 for the CTR case, the 16.71° and the 19.30° peaks resulted to correspond respectively to the 111 and the 200 Bragg peaks.

$$\sqrt{H^2 + K^2 + L^2} = \frac{a_{Au} Q}{2\pi} \tag{43}$$

In our experiment, all the observation for the range of temperature analysed showed no shift in the value of 2θ for the maxima of the peaks: hence we did not observe any kind of surface phase transition. The next Section aims to find a value for the uncertainty for both of the measurements in order to check whether they all agree or some don't quite match.

5.3 Error analysis

The error in Oleg Shpyrko's measurements was assumed to be originating only from obtaining the value of the maxima from the graph. His graphs plot intensity against momentum transfer q, and the following relation was assumed:

$$\frac{\Delta Q}{Q} = \frac{\Delta 2\theta}{2\theta} \tag{44}$$

The error in the momentum transfer was estimated to be ΔQ = 0.03 Å, and from this the uncertainty in 2θ was measured.

Error in the measurement of 2θ from our experiment was found by considering it equal to $\frac{1}{3}$ of the FWHM values obtained from Newplot when fitting the peaks. Table 5 shows the minimum and the maximum values of the diffraction angle generated for both the experiments.

$\mathbf{2\theta_{min}^{Shp}}$ (°)	$\mathbf{2\theta_{max}^{Shp}}$ (°)	**FWHM (Å)**	$\mathbf{2\theta_{min}^{Exp}}$ (°)	$\mathbf{2\theta_{max}^{Exp}}$ (°)	**Agree?**
6.57	6.95	X	6.78	6.78	Y
8.19	8.57	0.221889	8.34	8.48	Y
9.72	10.10	0.265597	9.87	10.05	Y
10.40	10.78	0.248439	10.53	10.69	Y
11.25	11.62	0.2761937	11.38	11.56	Y
13.35	13.73	0.2457253	13.58	13.74	Y
16.15	16.53	X	X	X	X
16.52	16.90	0.231489	16.63	16.79	Y
17.36	17.74	0.3408329	17.54	17.76	Y
17.74	18.12	0.183089	18.12	18.24	Y
X	X	0.263094	19.21	19.39	X
19.59	19.97	0.2424785	19.87	20.03	Y
20.13	20.51	0.1558079	20.48	20.58	Y
21.09	21.47	0.1541965	21.22	21.32	Y
21.51	21.89	0.1884375	21.83	21.95	Y
22.95	23.33	0.474586	23.27	23.59	Y
24.94	25.32	0.3910887	24.23	24.49	N

Table 5: **Table of errors for 2θ value of peaks, compared for the two different experiments**

Table 5 shows that all but the last peak match. We can therefore assume that the results from the two experiments are in full agreement. Some of the peaks are not observed in the other experiment; these mismatches can have different causes as it is briefly discussed in the previous Section.

6 Auger scans

The Auger scans are used to obtain the relative chemical composition of the surface. This tool differs from all the other techniques used so far, since it does not involve an x-ray beam, but a beam of electrons to probe the sample.

The theory behind Auger is very simple: low energy electrons are shone on the sample and as a consequence other electrons are emitted. These are collected by a detector that measures their energy. Knowing the initial energy of the incident electrons and their final energy of the ones detected we can easily obtain the binding energy of the electrons, (see Equation 45).

$$E_B = E_I - E_F \tag{45}$$

The binding energy is different for every material, hence a relative chemical composition can then be extracted.

Some Scanning Electron Microscope (SEM) images of the sample were taken after the experiment, and shown in Figure 24(a).

The SEM is a type of electronic microscope, which shines a focused beam of electrons onto the surface of a sample (it therefore uses electrons and not light waves, and the image is hence black and white, and insensitive of the chemistry of the sample).

Figure 24(a) shows a substrate with some drops of the diameter of around 2μm. Figures 24(b) and 24(c) show the Coherent X-ray Diffraction Imaging (CXDI) of one of the gold drops. This techniques probes the sample layer by layer using in-phase x-rays and the output is a 3D model of a feature (one of the drops in this case).

The substrate shown in Figure 24(a) can be made up either by pure silicon, or by a thin layer of gold on top of bulk silicon. These two models can be inspected with the use of the Auger scans obtained. Figure 25 shows three different Auger scans taken at different temperatures. The two big negative peaks indicate the contribution of gold and silicon: the left one is related to gold and the right one to silicon.

The ratio of the relative amount $\frac{Au}{Si}$ was obtained manually by taking the value for the minima for each observation. Auger scans measure the number of detected electrons N(E) as a function of kinetic energy: I then converted

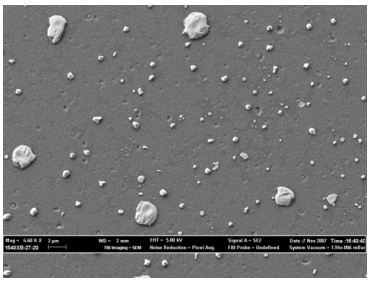

(a) SEM scan

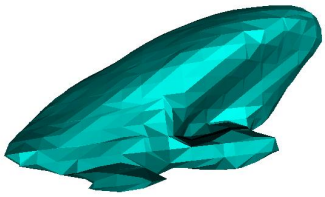

(b) 3D model of CXDI of a gold drop

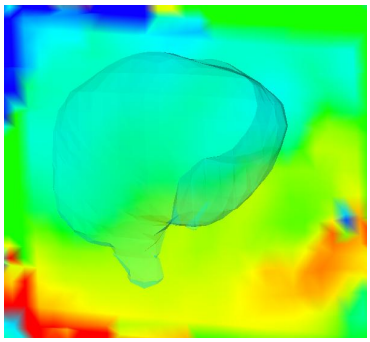

(c) CXDI of a gold drop

Figure 24: **Images of the sample**

these scans into more easily readable ones by taking a manual derivative and plotting dN(E).

Since the left peak describes the amount of gold at the very surface, we can see the realtive fraction of gold and silicon to decrease for the three different scans showed in Figure 25. The gold amount is at its maximum just after the deposition, and then it decreases as we melt. This result is clearly not surprising, since the liquid forms from both gold and silicon. The fact that we still see a very small peak on the frozen sample (blue line in Figure 25(c) and 25(d)) leads to the conclusion that the substrate is only formed by silicon, and the gold is present on the drops only: this is because gold occupies a much lower fraction of the surface compared with silicon.

Table 6 shows how the relative amount $\frac{Au}{Si}$ changes with temperature and time.

It is remarkable that on the frozen sample the gold occupies an even lower

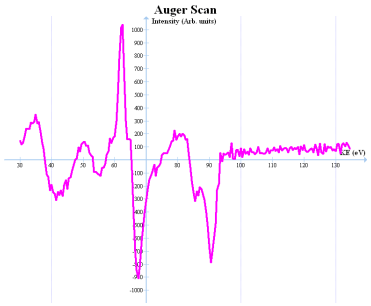

(a) Auger scan on cold sample just after the evaporation

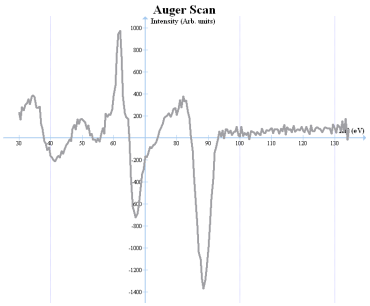

(b) Auger scan melted sample at around T=380°C

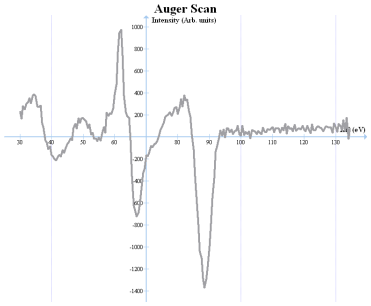

(c) Auger scan on newly frozen sample, at 347°C on heating up

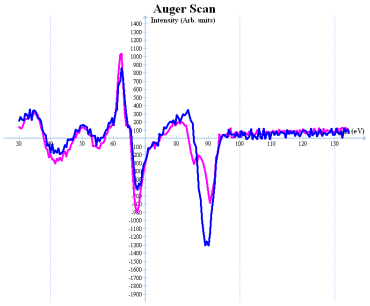

(d) Comparison between frozen sample just after the evaporation and after the manipulation

Figure 25: **Different Auger scans at various temperatures**

Scan number	**Temperature**	**Ratio $\frac{Au}{Si}$**	**Comments**
2	Room T	1.156289708	Just after deposition
3	330°C	0.649839376	
4	340°C	0.649379433	
5	362°C	0.523095144	
7	385°C	0.529239766	Melted
8	340°C	0.537296691	
11	347°C	0.481651376	Frozen (on heating)
12	Room T	1.898132428	Just after second deposition
13	367°C	0,797698945	

Table 6: **Different Auger scans reveal the relative presence of $\frac{Au}{Si}$ at the surface for different temperatures**

percentage of the surface compared to the melted sample.

When the gold is redeposited on the sample, it occupies most of the surface, even more than after the first deposition, as we expect, and as it is heated up the fraction diminishes.

7 Further observations

When the sample was extracted from the UHV chamber it showed a prominent line in the middle which was seen clearly also with the naked eye. This was probably caused by the continuous manipulation with synchrotron x-rays which heated up the sample where they were incident and ruined it.

This line can also be observed in the SEM images (see Figure 26).

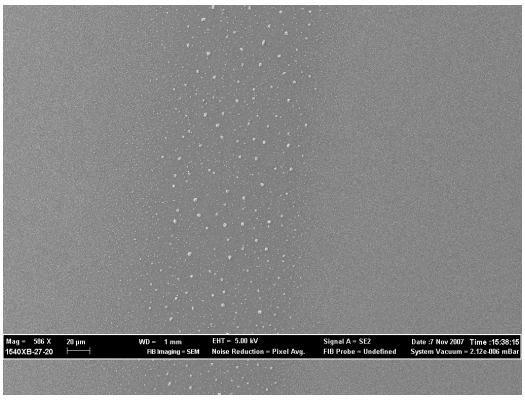

(a) SEM scan from far away

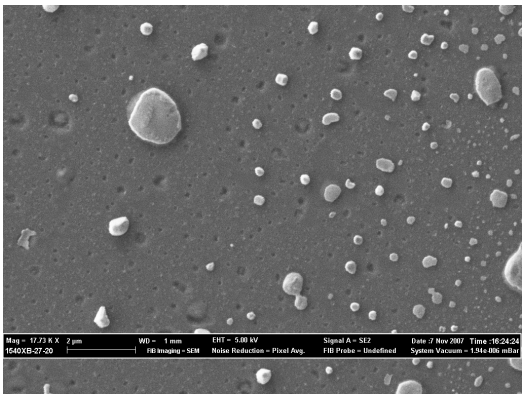

(b) Zoom on sample

Figure 26: **SEM images of the sample**

Figure 26(a) clearly shows the presence of a line, represented by wider gold drops. This is consistent with what is assessed above: the hotter part of the sample (where the x-ray beam was shone) is where the gold atoms are allowed to move most due to their higher entropy and therefore it shows

bigger drops. This is also seen in Figure 26(b), which is a zoom at the boundary between the line and the untouched sample.

This scan shows also the high roughness of the surface.

8 Discussion

This section aims to summarize the results obtained in the experiment, and draw some conclusions.

First of all, the presence of a eutectic in a geometry such as the one of our experiment was confirmed by the fact that a broad liquid peak was observed at 385°C. Being this temperature much lower than the melting point of either of the two elements in the sample, the presence of a liquid confirms the eutectic properties of gold and silicon. This particular eutectic was observed before by many other scientists (see for instance [4] and [5]), but the set up used in our experiment was considerably different from other ones previously inspected. The usual measurements involve the presence of an AuSi alloy, normally with a relative concentration of the two elements favourable to the formation of a eutectic.

The key difference is that in our experiment melting was only happening for few nanometres at the interface since the amount of gold evaporated was not enough to provide the melting of the whole sample: a liquid layer of mixed AuSi was sitting on a solid Si(100) bulk.

Melting was observed for the first time at 385°C, and the commonly accepted temperature for the formation of this eutectic is around 20°C lower (see Section 1.2). This mismatch can be caused by the fact that the thermocouple was attached to the tantalum clips. The eutectic takes place at the very surface, which is quite distant from the clips and this is therefore a source of error.

It is plausible that this distance causes a disagreement as high as 20°C, or even greater: last summer, in an internship taking place at the ESRF, I could experience this myself. My job was to calibrate the change in temperature caused by an increase in current passing through the sample clips, in order to obtain a calibration. This was inspected with the use of both a pyrometre and a thermocouple, and they gave quite different results. The thermocouple was attached to the clips (as in the real experiment) and the pyrometre was shone on the surface itself: for this reason it is much more likely that the measurements obtained by the pyrometre ware a better estimate of the temperature at the surface of the sample.

Another cause of this mismatch between theory and observation can be

the fact that even though in the experiment the increase in the current passing through the tantalum clips was done very slowly (in steps of 10°C usually, and then in steps of 5°C around the melting temperature), this was maybe not slowly enough for the sample to melt properly. This can be caused by the not common set up used in this experiment, i.e. the very low amount of gold compared with silicon.

However, this disagreement was not very worrying since our main interest was the consistency of the reading, which was proved to be invariant by another scan taken on the sample at a similar temperature (higher than 380°C), which showed that the sample was melting.

The GID scans showed evidence for supercooling, since melting was observed at a much higher temperature than freezing. On cooling down, the surface was measured to be semi-frozen at 340°C, and fully crystalline at around 330°C. Supercooling happens when the sample freezes at a lower temperature than it melts. This can be caused by the fact that we cooled down the sample fairly quickly, hence the sample at the interface did not have time to change state at a temperature similar to its melting point: the drop in the current was too fast. This could have caused the presence of an amorphous layer of gold and silicon in between the silicon bulk layer and the gold drops.

Some SEM images were taken on the sample two months after the experiment (see Sections 6 and 7), and a substrate with many drops on top were observed. The drops had a diameter going from around 20nm up to 2-3μm and may be formed by pure gold or by some amorphous AuSi mixture. They were caused by surface tension on the liquid sample and did not change in shape when the sample was frozen.

These images and the observation of supercooling intrigued us to understand what the composition of the substrate was, and two models were proposed. The first one assessed that the drops were sitting on a pure silicon surface, while the second one suggested that above the silicon bulk there was a layer of an amorphous mixture of gold and silicon.

Analysing the Auger scans taken during the experiment the first model was confirmed, and the silicon was shown to become increasingly important in the surface as the manipulations were made. This agrees with the SEM images which show that the drops, which are probably containing mostly

gold, occupy a much lower fraction of the surface compared to the substrate.

The SEM images showed a line of bigger drops in the middle of the sample, caused by the fact that the sample was heated up more than the rest of the surface at the spots where the x-ray was incident. Hence bigger drops were seen, due to their higher entropy. This feature was also visible with the naked eye and it is evidence of the x-ray ruining the sample.

Roughness was also observed in the SEM images as holes in the substrate, possibly formed by the drops sitting on it and then moving on heating the sample to join other drops to make a bigger one. The roughness was properly analysed in the CTR scans. The prediction was that it should increase as the temperature was increasing, and also as time was going on and as the sample was manipulated more and more. Change in the roughness is shown in a CTR scan as a decrease in intensity in between the Bragg peaks (in surface units the 101 and 103 for our case). The observations confirm the predictions, i.e. the sample becomes rougher as the time goes on, and, in particular, the roughest scan observed is the one at the highest temperature reached (473°C). When gold was re-evaporated on top of the sample, the roughness did not improve; this result is not surprising since the gold should deposit uniformally on top of the sample, hence not changing much the smoothness of the surface.

The measurements of the CTR scans had as the first objective to find a model for the structure at the interface. CTRs account for the structure of crystals, and since the gold sitting on the bulk is not a crystal but a powder, the model obtained counts for the interface and not for the surface, hence both gold and silicon have to be considered. This model was tried to be achieved in two ways: first manually, and then with the computer, using the ANAROD package. Manual scans were done in steps, starting from the simplest possible case (simple cubic bulk silicon) and improving the model gradually, considering a FCC silicon model, then accountin for gold, until the best model was reached. In this model the structure factor was considered to originate from a combination of diamond silicon bulk lattice (as it is in reality) and gold powder. The extra four atoms in the diamond structure were treated as a change in phase between the position of silicon and gold, coming from the fact that the gold could sit on top of one of these atoms.

In the last two models (which are the only ones that account for the

presence of gold) some parameter were adjusted to obtain the best possible fit. These parameters included the form factors of gold and silicon, and the distance z between the last silicon atom in the bulk and the first gold atom in the film. The ratio of the form factors $\frac{f_{Au}}{f_{Si}}$ was considered to account for the relative occupancy of the interface monolayer(s), taking f_{Si} to behave as a normalisation scale factor to adjust the measurements at the Bragg peaks. Since the form factor, which depends on the electron density, is often assumed to be equal to the atomic number of a given element, the ratio between the two for a total presence of gold in the first layer should be around 5.6 (coming from $Z_{Au} = 79$ and $Z_{Au} = 14$). The FCC model gives a very low percentage of gold at the interface (the form factor of silicon is found to be greater than the one of gold) and a distance $z = 0.55\ a_{Si}$. The model that accounts for diamond shows a negative gold form factor which results in a negative occupancy, which is clearly unphysical. What this means in fact is that the gold may not sit exactly on top of silicon atoms but be shifted slighly. The distance parameter in this case was $z = 0.33 a_{Si}$.

Since the models obtained manually were not perfect, we decided to use the ANAROD package to analyse further the CTRs. Two models were proposed, one involving only one atom in the surface (i.e. all gold atoms on the film were imagined to sit on top of each other), and the other one involving two atoms on the surface at different positions. All the combinations were tempted, and many of them were equivalent and they showed the same fit. The best fit with ANAROD was found to come from the first model, but the X^2 was enormously high (around 29). The parameters varied were analogous to the ones adjusted manually, corresponding to a scale factor, an occupancy parameter and a displacement parameter.

Further studies will be conducted on the CTRs in order to obtain a better fit. A possible improvement is to include also some silicon atoms on the surface file.

One of the possible reasons why the fits were not very good is that for a 100 diamond sample, in the presence of a step the 10L and the 01L sample are not equivalent, but they are asymmetric due to the presence of the four extra diamond atoms.

Another feature observed within the CTR scans is the presence of the 111 and 200 gold powder ring, at $L = 1.82$ and $L = 2.27$. These extra con-

tributions were another signature of the state of the sample at the interface, because liquid gold did not show such features, hence the scans where these peaks were observed were taken on a solid sample.

A contribution from the gold powder rings was also seen in the GID scans and their presence was one of the main hallmark of the solid state, together with the absence of the broad liquid peak. Our experiment was successful on reproducing the results obtained by Oleg Shpyrko on the observation of a crystalline layer on top of the melted surface. This was confirmed by the observation of surface Bragg peaks in the presence of the broad liquid peak caused by short range ordering. These peaks were seen to disappear at high temperature, around 473°C. These observation were discovered to be highly reproducible.

The diffraction angle at which these peaks were seen was compared between the two experiments, and all but three were found to match. Shpyrko's team did not observe evidence for the 19.30°C peaks, which corresponds to the 200 powder ring, and this means that in his case the bulk was fully liquid. He though sees a peak at 16.71°C, where the 111 powder ring appears. This probably means that there was another surface peak at that angle which was obscured by the powder ring. Moreover, we did not observe a peak at 16.34°C: this peak is also likely to have been hidden by the 111 powder ring. Only one angle (at around 25°C) was found to mismatch completely: that peak was observed in both the experiments, but at slighly different angles. Even accounting for the error in obtaining a proper value for Shpyrko's momentum tranfer the peaks did not agree. Moreover, the mismatch on the angles was found to increase as the angle increased: for high 2θ the angles agree very well but as 2θ increases the compatibility worsen.

Furthermore, the presence of a solid-solid surface phase transition was not observed, oppositely to what Shpyrko measured at 371°C as a shift in the momentum transfer of the surface peaks. In our case, the peaks were not moving, even for the scans at the highest temperatures.

Another tool used to proble the sample was the reflectivity. The reflectivity is closely related to the electron density variation as a function of height. The presence of a more dense thin film on top of silicon affects the reflectivity, and this fact allows the measurement of the thickness of the film.

Just after the first evaporation, the film was discovered to be 32Å thick,

but this value was observed to change with time, even though the sample was not heated up. It revealed an increase up to 39Å. This can be caused by a re-assessment of the silicon atoms and the gold atoms of some sort, which increases the hight of the unlayered sample (i.e. the film). As the temperature was increased, more and more activity was present at the interface and therefore the film was also seen to increase. The oscillations were observed to get fainter and fainter as the temperature was increased. As the eutectic point was approached, the scans showed more and more the shape of a non-uniform film, with oscillations only on the left of the plot.

Moreover, after the first melting, the oscillations were not observed anymore on the cold sample, to reappear only when the second deposition was carried out.

The error on measuring the thickness was mostly coming from the extrapolation of the minima of the oscillations, and as the oscillations were fainter as the temperature increased hence the error increased as well, up to a maximum value of around 6%.

9 Conclusion

In this experiment, the many techniques used were all aiming to investigate a different aspect of the changes on the sample as the temperature was increased. The reflectivity gave an insight of the amount of gold present on the surface, and how the non crystalline layer was varying with the changes in temperatures. CTR scans enabled us to track the changes at the interface between the crystal bulk and the thin film. Grazing Incident Diffraction was probing the state at the surface and its variation with temperature, keeping track of whether it was solid or liquid. Finally, Auger scans were measuring the relative chemical composition at the very surface of the sample.

To summarize, the main achievement of the experiment was the observation of an eutectic with such a thin film of gold on top of silicon (around $32\mathring{A}$ thick), and the observation of a crystalline surface sitting on top of a liquid interface. These results confirmed partially Oleg Shpyrko's observations, but not completely, since no surface phase transition was seen.

By the end of the experiment, the sample presented high roughness, and a silcon substrate (possibly mainly formed by silicon) with solid drops with a maximum diameter around 2μm sitting on top of it.

The experiment was overall successful, and future purposes of analysis mainly involve the achievement of a good model for the structure at the interface of the sample.

10 Acknowledgements

I first want to thank my supervisor, Ian Robinson, for giving me the possibility to work in Grenoble last summer which was a great experience, working in such an environment of friendship and science taught me a lot.

I really enjoyed working with him, both in Grenoble and throughout the year, he was very supportive and patient.

Secondly, I want to thank Roberto Felici, ID03 head scientist, and Thoms, the ID03 technician, for assisting me a lot in the summer internship and for the help we received during the experiment, which I found successful in many ways.

11 Bibliography

References

[1] D. McMorrow and J. Als-Nielsen, Elements of Modern X-ray Physics, Wiley & Sons (2001)

[2] C. Kittel, Introduction to solid state physics, Wiley & Sons, 8^{th} Edition (2005)

[3] I. K. Robinson and D. J. Tweet, Rep. Prog. Phys **55**, 599-652 (1992)

[4] O. G. Shpyrko et al., Science **313**, 77 (2006)

[5] O. G. Shpyrko et al., Phys. Rev. B **76**, 245436 (2007)

[6] P. Dutta, Current Science **78**, N^o 12 (2000)

[7] www.webelements.com

[8] www.ami.ac.uk

Further reading

- J. D. Verhoeven, Fundamentals of Physical Metallurgy, Wiley & Sons (1975)
- J. R. Hook & H. E. Hall Solid State Physics, Wiley & Sons, 2^{nd} Edition (1991)
- S. Kodambaka et al., Science **316**, 729 (2007)
- www.anl.gov
- Supporting online material of Oleg Shpyrko's research
- http://www.esrf.eu/computing/scientific/joint_projects/ANA-ROD/